

FGAP71 - December 18, 2020

Item # FGAP71 was discontinued on December 18, 2020 For informational purposes, this is a copy of the website content at that time and is valid only for the stated product.

PHOTODIODES

- ▶ GaP, Si, InGaAs, Ge, and Dual Band (Si/InGaAs) Detectors Available
- ▶ Available in TO Can, FC Connector, and Flat Wafer Body Styles
- ▶ Available in Hermetically Sealed Packages



[Hide Overview](#)

OVERVIEW

Features

- GaP, Si, InGaAs, Ge, and Dual Band (Si/InGaAs) Unmounted Photodiodes Available
- Wavelength Ranges from 150 to 2600 nm

Thorlabs stocks a wide selection of photodiodes (PD) with various active area sizes and packages. Discrete PIN junction photodiodes include indium gallium arsenide (InGaAs), gallium phosphide (GaP), and silicon (Si) materials. Germanium (Ge) photodiodes, which are based on an N-on-P structure, are also available.

Our fastest photodiodes are the FDS015, FDS02, and FDS025 Si photodiodes. The FDS015 Si photodiode has a 35 ps rise time and a 0.65 pF junction capacitance, making it the highest speed, lowest capacitance photodiode offered below. Alternatively, the FD11A Si photodiode has a dark current of 2 pA, making it our photodiode with the lowest dark current. The FGAP71, a GaP photodiode, is useful for detection of UV light sources from 150 to 550 nm. The FD10D and FD05D are InGaAs photodiodes with high responsivity from 900 to 2600 nm, allowing detection of wavelengths beyond the normal 1800 nm range of typical InGaAs photodiodes. The DSD2 is a dual-band photodiode, which incorporates two photodetectors sandwiched on top of each other (Si substrate on top of an InGaAs substrate), offering a combined wavelength range of 400 to 1700 nm.

To complement our photodiode product line, we offer mounted photodiodes and a range of compatible photodiode sockets. Please note that the PDs sold below are not calibrated, meaning responsivity will differ slightly from lot to lot; refer to the *Response Variation* tab for more information. We also offer calibrated photodiodes, which come with with NIST-traceable calibration, to correct for the differences in responsivity. Many of our photodiodes can be reverse voltage biased using the PBM42 DC Bias Module for faster speed and higher optical power detection.

For information on the photodiode saturation limit and the noise floor, as well as a collection of Thorlabs-conducted experiments regarding spatial uniformity (or varying responsivity) and dark current as a function of temperature, refer to the *Lab Facts* tab. This tab also outlines the theory and methods we use to define the specifications of our photodiodes. For example, the Noise Equivalent Power (NEP) as a Function of Temperature section provides background on NEP values specified by shot noise and thermal noise. With zero bias (Photovoltaic Mode), the NEP is specified by the thermal noise only, which is caused by the shunt resistance of the photodiode. The *Photodiode Tutorial* provides more general information regarding the operation, terminology, and theory of photodiodes.

Mounted and Unmounted Detectors

Unmounted Photodiodes (150 - 2600 nm)
Calibrated Photodiodes (350 - 1800 nm)
Mounted Photodiodes (150 - 1800 nm)
Thermopile Detectors (0.2 - 15 μm)
Photovoltaic Detectors (2.0 - 10.6 μm)
Pigttailed Photodiodes (320 - 1000 nm)

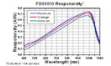
Inhomogeneity on the edge of an active area of the detector can generate unwanted capacitance and resistance that distorts the time-domain response of a photodiode. Thorlabs therefore recommends that the incident light on the photodiode is well centered on the active area. This can be accomplished by placing a focusing lens or pinhole in front of the detector element.

Thorlabs offers spectral-flattening filters that are designed to improve the response uniformity of our silicon photodiodes. [Click here to learn more.](#)

[Hide Response Variation](#)

RESPONSE VARIATION

The responsivity of a particular photodiode varies from lot to lot. Due to this, the photodiode you receive may have a slightly different response than what is represented below. For example, to the right, a graph for the FDS1010 photodiode shows the extent that the response may vary. This data was collected from 104 photodiodes. Minimum, Average, and Maximum responsivity was calculated at each data point and has been plotted.



[Click to Enlarge](#)

To view typical responsivity vs. wavelength data for each individual photodiode, please click the  buttons in the product specifications tables below.

[Hide Photodiode Tutorial](#)

PHOTODIODE TUTORIAL

Photodiode Tutorial

Theory of Operation

A junction photodiode is an intrinsic device that behaves similarly to an ordinary signal diode, but it generates a photocurrent when light is absorbed in the depleted region of the junction semiconductor. A photodiode is a fast, highly linear device that exhibits high quantum efficiency based upon the application and may be used in a variety of different applications.

It is necessary to be able to correctly determine the level of the output current to expect and the responsivity based upon the incident light. Depicted in Figure 1 is a junction photodiode model with basic discrete components to help visualize the main characteristics and gain a better understanding of the operation of Thorlabs' photodiodes.

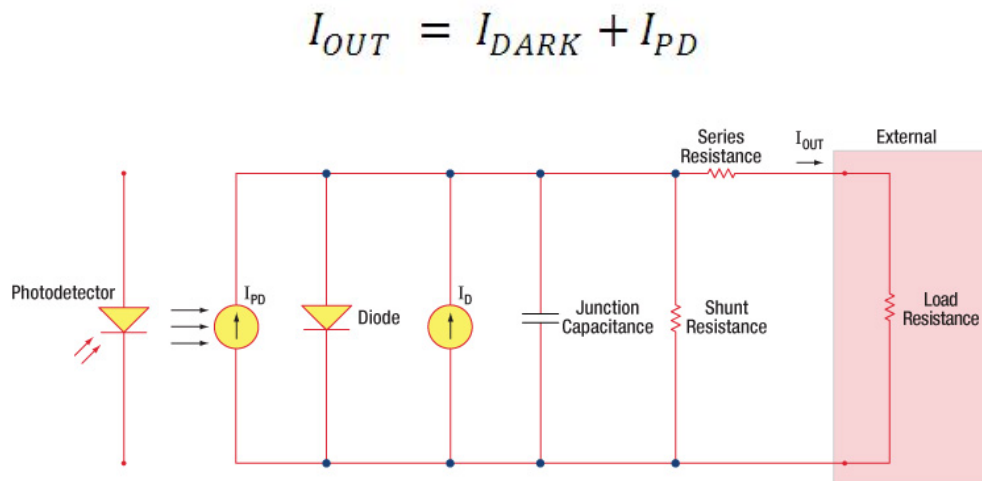


Figure 1: Photodiode Model

Photodiode Terminology

Responsivity

The responsivity of a photodiode can be defined as a ratio of generated photocurrent (I_{PD}) to the incident light power (P) at a given wavelength:

$$R(\lambda) = \frac{I_{PD}}{P}$$

Modes of Operation (Photoconductive vs. Photovoltaic)

A photodiode can be operated in one of two modes: photoconductive (reverse bias) or photovoltaic (zero-bias). Mode selection depends upon the application's speed requirements and the amount of tolerable dark current (leakage current).

Photoconductive

In photoconductive mode, an external reverse bias is applied, which is the basis for our DET series detectors. The current measured through the circuit indicates illumination of the device; the measured output current is linearly proportional to the input optical power. Applying a reverse bias increases the width of the depletion junction producing an increased responsivity with a decrease in junction capacitance and produces a very linear response. Operating under these conditions does tend to produce a larger dark current, but this can be limited based upon the photodiode material. (Note: Our DET detectors are reverse biased and cannot be operated under a forward bias.)

Photovoltaic

In photovoltaic mode the photodiode is zero biased. The flow of current out of the device is restricted and a voltage builds up. This mode of operation exploits the photovoltaic effect, which is the basis for solar cells. The amount of dark current is kept at a minimum when operating in photovoltaic mode.

Dark Current

Dark current is leakage current that flows when a bias voltage is applied to a photodiode. When operating in a photoconductive mode, there tends to be a higher dark current that varies directly with temperature. Dark current approximately doubles for every 10 °C increase in temperature, and shunt resistance tends to double for every 6 °C rise. Of course, applying a higher bias will decrease the junction capacitance but will increase the amount of dark current present.

The dark current present is also affected by the photodiode material and the size of the active area. Silicon devices generally produce low dark current compared to germanium devices which have high dark currents. The table below lists several photodiode materials and their relative dark currents, speeds, sensitivity, and costs.

Material	Dark Current	Speed	Spectral Range	Cost
Silicon (Si)	Low	High Speed	Visible to NIR	Low
Germanium (Ge)	High	Low Speed	NIR	Low
Gallium Phosphide (GaP)	Low	High Speed	UV to Visible	Moderate
Indium Gallium Arsenide (InGaAs)	Low	High Speed	NIR	Moderate
Indium Arsenide Antimonide (InAsSb)	High	Low Speed	NIR to MIR	High
Extended Range Indium Gallium Arsenide (InGaAs)	High	High Speed	NIR	High
Mercury Cadmium Telluride (MCT, HgCdTe)	High	Low Speed	NIR to MIR	High

Junction Capacitance

Junction capacitance (C_j) is an important property of a photodiode as this can have a profound impact on the photodiode's bandwidth and response. It should be noted that larger diode areas encompass a greater junction volume with increased charge capacity. In a reverse bias application, the depletion width of the junction is increased, thus effectively reducing the junction capacitance and increasing the response speed.

Bandwidth and Response

A load resistor will react with the photodetector junction capacitance to limit the bandwidth. For best frequency response, a 50 Ω terminator should be used in conjunction with a 50 Ω coaxial cable. The bandwidth (f_{BW}) and the rise time response (t_r) can be approximated using the junction capacitance (C_j) and the load resistance (R_{LOAD}):

$$f_{BW} = 1 / (2 * \pi * R_{LOAD} * C_j)$$

$$t_r = 0.35 / f_{BW}$$

Noise Equivalent Power

The noise equivalent power (NEP) is the generated RMS signal voltage generated when the signal to noise ratio is equal to one. This is useful, as the NEP determines the ability of the detector to detect low level light. In general, the NEP increases with the active area of the detector and is given by the following equation:

$$NEP = \frac{\text{Incident Energy} * \text{Area}}{\frac{S}{N} * \sqrt{\Delta f}}$$

Here, S/N is the Signal to Noise Ratio, Δf is the Noise Bandwidth, and Incident Energy has units of W/cm^2 . For more information on NEP, please see Thorlabs' Noise Equivalent Power White Paper.

Terminating Resistance

A load resistance is used to convert the generated photocurrent into a voltage (V_{OUT}) for viewing on an oscilloscope:

$$V_{OUT} = I_{OUT} * R_{LOAD}$$

Depending on the type of the photodiode, load resistance can affect the response speed. For maximum bandwidth, we recommend using a 50 Ω coaxial cable with a 50 Ω terminating resistor at the opposite end of the cable. This will minimize ringing by matching the cable with its characteristic impedance. If bandwidth is not important, you may increase the amount of voltage for a given light level by increasing R_{LOAD} . In an unmatched termination, the length of the coaxial cable can have a profound impact on the response, so it is recommended to keep the cable as short as possible.

Shunt Resistance

Shunt resistance represents the resistance of the zero-biased photodiode junction. An ideal photodiode will have an infinite shunt resistance, but actual values may range from the order of ten Ω to thousands of $M\Omega$ and is dependent on the photodiode material. For example, an InGaAs detector has a shunt resistance on the order of 10 $M\Omega$ while a Ge detector is in the $k\Omega$ range. This can significantly impact the noise current on the photodiode. For most applications, however, the high resistance produces little effect and can be ignored.

Series Resistance

Series resistance is the resistance of the semiconductor material, and this low resistance can generally be ignored. The series resistance arises from the contacts and the wire bonds of the photodiode and is used to mainly determine the linearity of the photodiode under zero bias conditions.

Common Operating Circuits

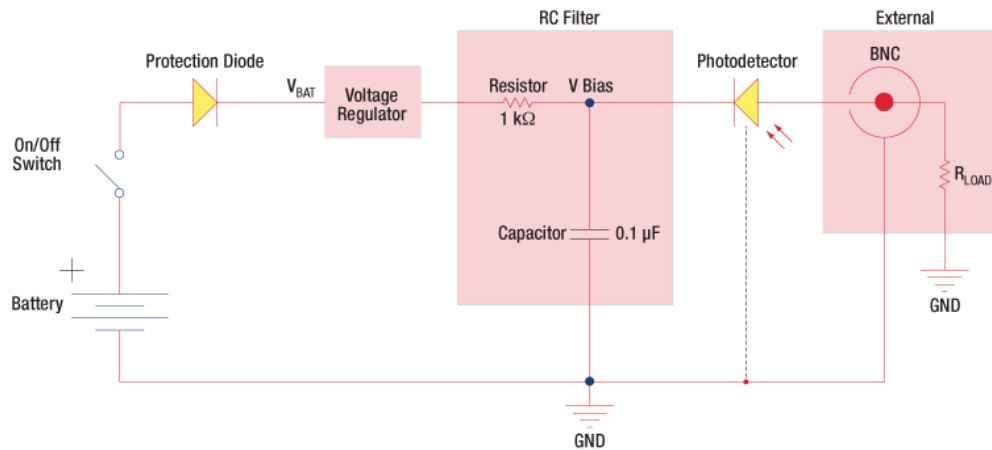


Figure 2: Reverse-Biased Circuit (DET Series Detectors)

The DET series detectors are modeled with the circuit depicted above. The detector is reverse biased to produce a linear response to the applied input light. The amount of photocurrent generated is based upon the incident light and wavelength and can be viewed on an oscilloscope by attaching a load resistance on the output. The function of the RC filter is to filter any high-frequency noise from the input supply that may contribute to a noisy output.

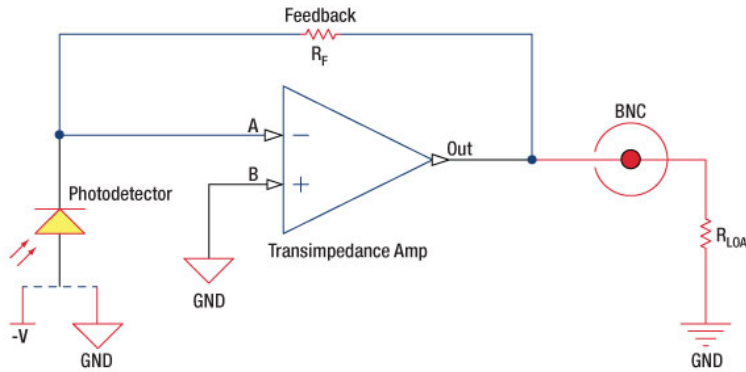


Figure 3: Amplified Detector Circuit

One can also use a photodiode with an amplifier for the purpose of achieving high gain. The user can choose whether to operate in Photovoltaic or Photoconductive modes. There are a few benefits of choosing this active circuit:

- Photovoltaic mode: The circuit is held at zero volts across the photodiode, since point A is held at the same potential as point B by the operational amplifier. This eliminates the possibility of dark current.
- Photoconductive mode: The photodiode is reverse biased, thus improving the bandwidth while lowering the junction capacitance. The gain of the detector is dependent on the feedback element (R_f). The bandwidth of the detector can be calculated using the following:

$$f(-3dB) = \sqrt{\frac{GBP}{4\pi * R_f * C_D}}$$

where GBP is the amplifier gain bandwidth product and C_D is the sum of the junction capacitance and amplifier capacitance.

Effects of Chopping Frequency

The photoconductor signal will remain constant up to the time constant response limit. Many detectors, including PbS, PbSe, HgCdTe (MCT), and InAsSb, have a typical $1/f$ noise spectrum (i.e., the noise decreases as chopping frequency increases), which has a profound impact on the time constant at lower frequencies.

The detector will exhibit lower responsivity at lower chopping frequencies. Frequency response and detectivity are maximized for

$$f_c = \frac{1}{2\pi\tau_r}$$

LAB FACTS

[Hide Lab Facts](#)

Summary

This tab contains a collection of experiments performed at Thorlabs regarding the performance of photodiodes we offer. Each section is its own independent experiment, which can be viewed by clicking in the appropriate box below. *Photodiode Saturation Limit and Noise Floor* explores how different conditions, including temperature, resistivity, reverse-bias voltage, responsivity, and system bandwidth, can affect noise in a photodiode's output. *Photodiode Spatial Uniformity* explores variations in the responsivity as a small-diameter light beam is scanned across the active area of the photodiode. Photodiodes with different material compositions are tested, and eight units of one silicon-based model are tested to investigate unit-to-unit variations. *Dark Current as a Function of Temperature* and *Noise Equivalent Power (NEP) as a Function of Temperature* describe how dark current and NEP, respectively, vary with temperature and how measurements are affected. *Beam Size and Photodiode Saturation* shows how the photodiode saturation point changes with the incident beam size and investigates several models to explain the results. *Bias Voltage* examines the effects of incident power on the effective reverse bias voltage of a photodiode circuit and verifies a reliable model for predicting those changes.

Photodiode Saturation Limit and Noise Floor

We present laboratory measurements of the saturation limit and noise floor of a Thorlabs silicon photodiode. While all photodiodes function similarly, there are a number of parameters that affect the noise floor and saturation limit of a photodiode including the sensor temperature, resistivity, reverse bias voltage, responsivity, and system bandwidth. Here we investigated the effect of reverse bias voltage and load resistance within a silicon-based photodiode detection system. Increasing the reverse bias increased the saturation limit and had minimal effect on the noise floor. Decreasing the load resistance decreased the noise floor until reaching the noise of the measurement system, but also decreased the saturation limit. These results demonstrate some of the considerations necessary for choosing the reverse bias voltage and load resistance, and emphasize that noise sources within all of the components must be considered when creating a detection system.

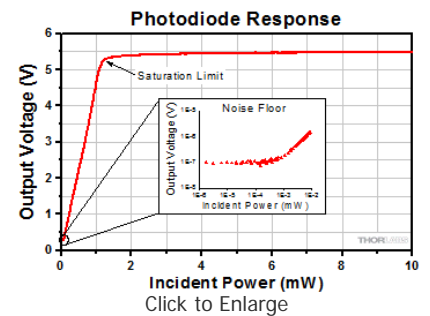


Figure 1. Overview of the Photodiode's Response Curve, Highlighting the Saturation Limit and the Noise Floor

For our experiment we used the FDS100 Si Photodiode as the photodiode under investigation. The collimated output of a fiber-pigtailed laser diode was used as the light source with output power from 0 to 50 mW. The collimated beam was incident upon a beamsplitter that transmitted the majority of the light to the photodiode under investigation and reflected the rest towards a reference power sensor. The photodiode response was then evaluated under various resistive loads and with different reverse bias voltages.

Lab Facts

Click for full Lab Facts summary

The plots to the right and below summarize the measured results for the various tested configurations. From these graphs the changes to the photodiode's linear response, noise floor, and saturation limit can be observed under different reverse voltage biases and load resistances. Figure 1 provides an overview of the photodiode response with a reverse voltage bias of 5 V and resistive load of 10 kΩ. The photodiode saturated at the upper limit of the response when the output photovoltage approached the reverse bias voltage. The noise floor at the lower limit of the response was a result of dark current and the thermal noise from the resistive load (Johnson noise). Figure 2 summarizes the results obtained using the photodiode with a 1 kΩ resistive load and various reverse bias voltages. It illustrates that the saturation limit can be raised by increasing the reverse bias voltage (within specification). Figure 3 summarizes the results from using the photodiode with a 5 V reverse bias voltage and various resistive loads. It illustrates that the slope of the photovoltage response increased as the load resistance was increased. Figure 4 summarizes the noise floor results obtained using a 0 V reverse bias voltage and various resistive loads. The noise floor increased when larger load resistances were used. It is important to note that the 1 kΩ data was measured above the theoretical Johnson noise due to the voltage noise within the measurement system. Minimal change in the overall noise floor was seen when using a 5 V reverse bias voltage. For details on the experimental setup employed and these summarized results, please click here.

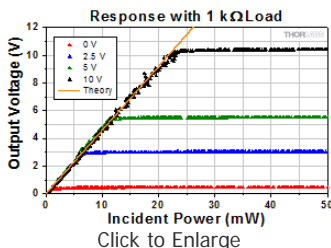


Figure 2. Photovoltage Dependence on Reverse Bias Voltage

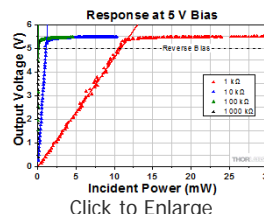


Figure 3. Response with Various Resistive Loads

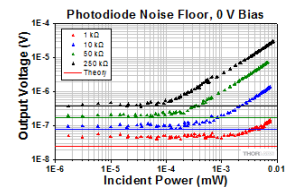


Figure 4. Noise Floor with Various Resistive Loads

[Hide Spatial Uniformity](#)

SPATIAL UNIFORMITY

Do all regions of a photodiode's active area have the same responsivity?

The output signal strength from a photodetector is significantly affected by the optical power and wavelength of the incident light. A measure of this relationship is responsivity, which is the magnitude of the output photocurrent divided by the optical power of the incident light. While responsivity has units of ampere per watt, it also varies with wavelength. Often overlooked is that responsivity can also vary as different regions of the photodiode's active area are illuminated.

This work investigated the change in photodetector response as a light beam, with a diameter that was small in comparison to the active area of the photodiode, was scanned across the active area. A selection of photodetectors, based on mounted gallium phosphide (GaP), silicon (Si), indium gallium arsenide (InGaAs), or

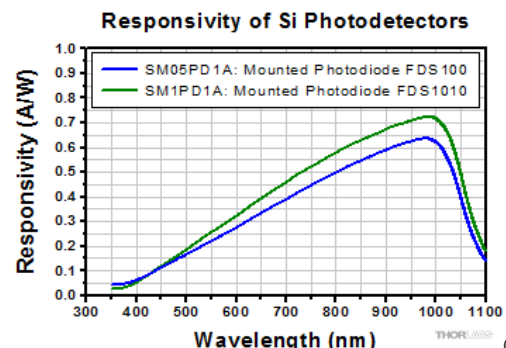


Figure 1: Responsivity, which describes the relationship between the strength of the photocurrent output by the photodetector and the optical power in the incident beam, is dependent on the wavelength

germanium (Ge) photodiodes, were tested.

of the incident light.

Responsivity is Wavelength Dependent^{1,2}

One reason responsivity varies with respect to wavelength is the relationship among optical power, wavelength, and photo-generated electrons. A light beam illuminating a surface provides an optical power equal to the energy in the beam divided by the time the surface was illuminated. The energy in a single-wavelength beam equals the number of incident photons times the energy of a single photon. Decreasing the wavelength of the light increases the energy of the photons. If the wavelength is decreased, but the optical power is kept the same, there are fewer incident photons.

A single photon can generate no more than a single electron of photocurrent in these photodetectors. Due to this, reducing the wavelength of the incident light while holding its optical power constant results in a reduced photocurrent. Since responsivity relates the output photocurrent to the incident optical power, instead of to the number of incident photons per unit time, responsivity is lower at lower wavelengths. The responsivity curves plotted in Figure 1 are examples showing responsivity increasing with wavelength.

The upper wavelength of a photodetector's responsivity is limited by inherent properties of the semiconductor material. In order for an incident photon to contribute to the photocurrent, the photon must have enough energy to free an electron from its bonds to its host atom. Photons with wavelengths above the upper wavelength limit do not have enough energy. The semiconductor material composing the photodiode determines the wavelength of this limit.

Response May Vary as Different Regions of the Photodiode's Active Area are Illuminated^{1,2}

An electron that has escaped the bonds of its host atom by absorbing the energy of a photon is a photo-generated electron. A photo-generated electron contributes to the photocurrent only if the electron is able to successfully travel from where it was generated, across the semiconductor material, and to an electrical contact. A photo-generated electron does not contribute to the photocurrent if it is re-absorbed by the semiconductor material before reaching a contact, which is a more likely outcome if the electron encounters a defect.

Defects are places where the semiconductor's crystal lattice is not perfect. These locations include dislocations, impurities, and voids in the crystal lattice. The external surfaces of a real crystal with finite dimensions are also imperfections, since a perfect crystal is infinite in length, height, and width. Defects in the semiconductor crystal absorb photo-generated electrons at a high rate and turn their kinetic energy into heat, rather than allow the electrons to contribute to the photocurrent.

Electrons generated near defects are more likely to be re-absorbed and less likely to contribute to the photocurrent. While the density of defects in a semiconductor can be minimized, the semiconductor crystals used in photodiodes are not perfect. It is also not unusual for the density of defects to vary throughout the volume of the semiconductor crystal, as well as for the growth of some semiconductor materials to be more prone to forming defects than others.

If the density of defects varies throughout the volume of the semiconductor material, the magnitude of the photocurrent generated within each region would be expected to be different. Since the photodetector's responsivity depends on the magnitude of photocurrent, a varying density of defects would result in the responsivity changing as different locations on the photodetector are illuminated. This effect was investigated using the procedure described in the following section.

Experimental Setup and Results

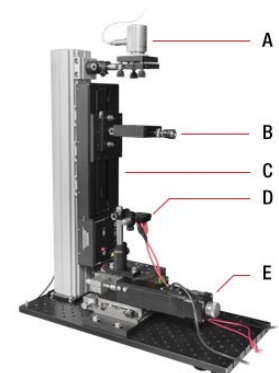
Measurement Objectives

Several photodetectors were tested to investigate the uniformity of the responsivity across their active areas. The spatially dependent responsivities of one GaP-based, four Si-based, two InGaAs-based, and two Ge-based photodetectors were measured at selected wavelengths. Testing was conducted to investigate the spatial uniformity of the responsivity of:

- All nine photodetector models at a wavelength close to the wavelength of peak responsivity. (Results contained in the first expandable table below.)
- A Si-based, an InGaAs-based, and a Ge-based photodetector at three different wavelengths. (Results contained in the second expandable table below.)
- Eight different units of a single Si-based photodetector model at a wavelength close to the wavelength of peak responsivity. (Results contained in the third expandable table below.)

Experimental Setup (Components Labeled in Figure 2 are Labeled in the Following)

The experimental setup consisted of a light source (not shown) that was fiber-coupled to an RC12APC-P01 collimator (A), which was installed in a KM100T kinematic mount. An AC254-150-A achromatic doublet lens with a 150 mm focal length (B), which was installed in a ST1XY-D mount, focused the light on the active area of the photodetector (D), which was mounted with the help of a KB1P magnetic quick-release carriage set. Other components in the vertical arm included an LTS150 motorized linear translation stage (C), an XT66P1 vertical mounting plate, an XT66-500 66 mm construction rail, and four XT66C4 clamping platforms. The components in the horizontal arm included two previous-generation LNR50S motorized linear translation stages (E), an LNR50P3 XY adapter



Click to Enlarge

Figure 2: The setup used to measure the change in response across the active area of each photodiode included: a reflective collimator (A), an achromatic doublet lens (B), vertically-mounted linear translation stage (C), the photodetector under test (D), and two horizontally-mounted translation stages (E) of which one is visible.

plate, a baseplate, and two BSC201 closed-loop stepper motor controllers (not shown), which scanned the beam across the active area of the photodetector (D). Most light sources were products from our Superluminescent Diode series. The exception was the 405 nm light source, which was an S3FC405 benchtop laser source.

Procedure

The diameter of the beam was scaled according to the active area of the photodetector, so that approximately 3600 measurements were taken in a 60 x 60 grid across the surface of each photodiode. The beam diameter used for each photodiode was between 50 μm and 500 μm , and the size used to make a particular measurement is included in the notes that accompany each plot in the following expandable tables. To view this information, click on the plot of interest.

During the scan, the position of the beam remained stationary, and the two LNR50S motorized stages were used to translate the photodetector in the two directions perpendicular to the optic axis. To ensure that the entire active area of the photodetector was tested, the dimensions of the scan area exceeded the dimensions of the active area.

No reverse bias voltage was applied to any of the photodiodes during this investigation.

Results (Click More [+] to Expand the Following Tables, and Click Less [-] to Hide Them)

The measurement data were normalized and then plotted with respect to the measurement position. The data in each measurement set were normalized with respect to the value at the center of the active area, which resulted in plots that show the variation of the responsivity across each photodetector's active area and allow the results from these nine different photodetector models to be compared. The plotted data were also processed to remove data points with values indistinguishable from noise. This was done to eliminate data points corresponding to measurements made outside of the active area of each photodetector. However, this approach also removed some measurements made within, but close to, the outer edges of the active areas. The lower photocurrent generated by these regions may have been due to the beam spot partially illuminating regions outside of the active area, as well as photocurrent suppressed by a higher density of defects near the edges.

The plots can be revealed by expanding the following tables. Each plot includes a dashed outline surrounding the central 90% of the active area of the photodiode. Under general use, the light beam should remain within this central 90% region to avoid edge effects. Click on each plot to reveal information about the active area of the photodiode and the size of the beam scanned across the active area.

Since these photodetectors represent a small sample size, these measurements are representative of the other photodetectors of its model, but results obtained using other units of the same model may vary. The measurements acquired for these photodetector units were repeatable, but no two semiconductor crystals are identical and unit-to-unit variations should be expected. The following tables show that:

- **First Table:** The variations of the responsivities across the active areas of the Ge-based and GaP-based photodetectors are greater than the variations of the responsivities across the active areas of the Si-based and InGaAs-based photodetectors. This suggests the defect densities of the Si-based and InGaAs-based semiconductor materials are more uniform than the defect densities of the Ge-based and GaP-based semiconductor materials.
- **Second Table:** The variations of the responsivities across the active areas of a Si-based, an InGaAs-based, and a Ge-based photodetector change with wavelength. For each photodetector, the minimum spatial variations of the responsivity occurred when the wavelength of light was near the wavelength of the peak value of responsivity.
- **Third Table:** Eight units of a single Si-based photodetector model had similar variations of spatial uniformity across their active areas.

1) All Nine Photodetectors: Uniformity of Response to Light with Near Peak Responsivity Wavelength

2) Selected Si-, InGaAs-, and Ge-Based Photodetectors: Uniformity of Response of Each to Three Different Wavelengths of Light

3) Eight Si-Based SM1PD2A Photodetectors: Uniformity of Response to Light Near Peak Responsivity Wavelength Compared

References

- [1] G. P. Agrawal, *Fiber-Optic Communication Systems*, 2nd ed., John Wiley & Sons, Inc., New York, 1997. (Particularly Chapter 4)
- [2] A. Rogalski, K. Adamiec, and J. Rutkowski, *Narrow-Gap Semiconductor Photodiodes*, SPIE Press, Bellingham, WA, 2000.

DARK CURRENT

Dark Current as a Function of Temperature

Measurements of dark current as a function of temperature were acquired for several unmounted photodetectors. As is described in the following section, dark current is a relatively small electrical current that flows in p-n junction photodetectors when no light is incident on the detector. Measurements were taken for silicon (Si), germanium (Ge), gallium phosphide (GaP), and indium gallium arsenide (InGaAs) reverse-biased photodiodes over temperatures from 25 °C to approximately 55 °C.

Current-Voltage Characteristics of p-n Junction Photodiodes

The characteristic current-voltage relationship of p-n junction photodiodes, as diagrammed in Figure 1, possesses forward-biased and reverse-biased voltage regimes. In the reverse-biased voltage regime, in which p-n junction photodiodes are operated, a potential difference applied across the diode resists the flow of current. Ideally, if no light is incident on a reverse-biased photodiode, no current flows.

Under real-world conditions, random processes in the semiconductor material of the photodiode always generates current carriers (electrons and holes) that produce current. These current generation processes are not driven by the photogeneration of electrons and holes. Instead, they are largely driven by the thermal energy contained in the semiconductor material.[1] This dark current is generally small, but it is present when the photodiode is reverse biased and not illuminated. Dark current magnitudes vary for photodiodes of different material compositions; the efficiencies of the thermal generation processes depend on the type and crystal quality of the semiconductor used in the detector's sensing head. The magnitude of the dark current can be expected to increase as the temperature of the photodiode increases.

When a photodiode is illuminated, the current generated by the incident light adds to the dark current. The carriers in the photocurrent are generated by the energy contained in the photons of the incident light. Above a certain illumination threshold intensity, the magnitude of the photocurrent exceeds the magnitude of the dark current. When the photocurrent is larger than the dark current, the magnitude of the photocurrent can be calculated by measuring the total current and then subtracting the contribution of the dark current. When the photocurrent is smaller than the dark current, the photocurrent is undetectable. Because of this, it is desirable to minimize the levels of dark current in photodiodes.

For convenience, both dark current and photocurrent are discussed as being independent of voltage over a range of voltages when the photodiode is reverse biased; however, the current flowing in real-world reverse-biased photodetectors is not completely independent of voltage over any voltage range. Regardless of whether the diode is illuminated, the current will increase as the magnitude of the reverse-bias voltage increases. In addition, if the reverse-bias voltage is increased beyond a certain threshold, the photodiode will suffer reverse breakdown, in which the magnitude of the current increases exponentially and permanent damage to the diode is likely.

Experiment: Dark Currents Measured for Packaged Photodiodes

Dark currents were measured over temperatures of 25 °C to approximately 55 °C for four representative unpackaged photodiodes: the Si-based FDS1010, the Ge-based FDG50, the GaP-based FGAP71, and the InGaAs-based FGA10.

Experimental Setup

The experimental setup was designed to ensure a constant reverse-bias voltage across the photodiode, control the temperature of the detector, block light from reaching the detector, and establish an electrical path between the detector and the Keithley 6487 ammeter that isolated the measured current from extraneous electromagnetic interference (EMI) noise sources. Dark currents for these detectors can be on the order of nA, which made it important to control these conditions to ensure accurate measurements.

The detector enclosure consisted of a pair of nested aluminum metal boxes, which are shown with their covers off in Figure 2. Only one box would be required to create a light-tight environment for the photodiode, but an outer box was included in the setup to shield the inner box from EMI. The detector was placed inside the inner box, and it was electrically connected to the Keithly 6487 ammeter. The ammeter provided the required 5 V reverse-bias and received the output current

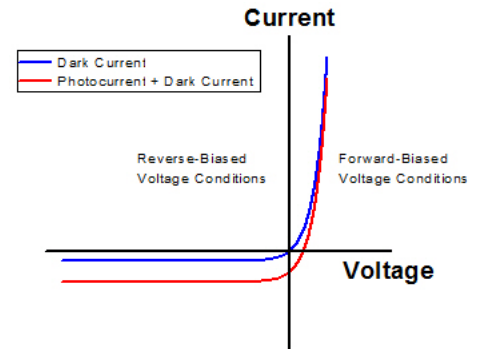
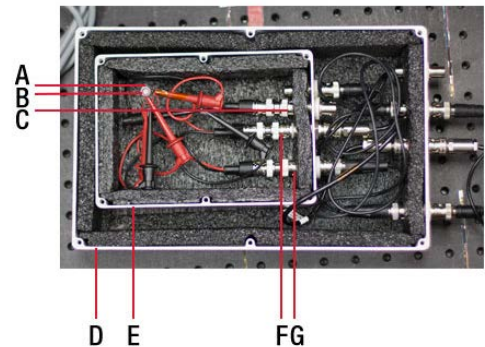


Figure 1: Current-Voltage Characteristic of a P-N Junction



[Click to Enlarge](#)

signal. The electrical signals between the ammeter and the photodiode were routed through the two boxes using a combination of cables and feedthroughs. The 5 V bias voltage was connected to the photodiode using coax cables and BNC-to-BNC feedthroughs in the walls of both metal boxes. The current signal from the photodiode was connected to the BNC end of a BNC-to-Triax feedthrough integrated into the wall of the inner box. The signal was then routed through the outer box and to the Keithly 6487 using triax cables and a Triax-to-Triax feedthrough in the outer box. Triax cables were used because coax cables are poorly shielded, and using a coax cable to route the signal to the ammeter could introduce noise from EMI sources to the signal read from the detector. As the outer box shields the inner box from EMI, the noise introduced on the signal as it travels from the detector to the BNC-to-Triax feedthrough is mitigated.

Thermistors were used to monitor the temperatures of each photodiode continuously during the experiment. A piece of thermal tape was used to hold the thermistor flush against the TO cans of the FDG50, FGAP71, and the FGA10 during testing. The photosensor of the FDS1010 is mounted on a ceramic substrate, and when it was tested the thermistor was taped to the back of the substrate. The electrical connection between the thermistor and TSP01 temperature logger was performed using BNC cables, BNC-to-BNC bulkhead feedthroughs to route the signal out of the nested boxes, and a custom BNC-to-phono jack cable to connect to the temperature logger.

A custom temperature chamber based on a XE25C9 standard enclosure was used to conduct these tests. It is shown on top of the cart in Figure 3. The enclosure had a floor and four walls, and insulation was attached to all inner and outer surfaces. A lid for the enclosure was fashioned from a sheet of hardboard bordered with XE25 rails, and insulation was attached to the inner surface of the hardboard. Six resistive foil heaters were affixed to the walls of the XE25C9 enclosure, and they were driven using the PRO8000 fitted with six TED8040 thermoelectric cooler (TEC) controller cards placed on the bottom shelf of the cart in Figure 3. Each TED8040 was interfaced with a heater and a thermistor installed in the chamber. The reading from the thermistor determined the current sent to drive the heater. The chamber was not actively cooled; cooling was instead performed by withdrawing the current driving the heaters and, as an option, opening the lid of the chamber.

The TED8040 units are designed to be interfaced with TECs, which produce heat when current flows in one direction, and which provide cooling when the current flows in the opposite direction. Because of this, when the enclosure exceeded the setpoint temperature, the TED8040 units in this experimental setup did not cut off the driving current. They instead reversed the current flow in an effort to produce cooling. In contrast to TECs, resistive foil heaters generate heat regardless of the direction of current flowing through them. In order to divert the driving current from the heaters, an electrical circuit, diagrammed in Figure 4, that included two rectifying diodes was designed and implemented. Rectifying diodes allow current to flow only in one direction. When the temperature reading from the thermistor was lower than the setpoint temperature, current flowed in the direction of the red arrows and through the resistive heater, and heat was generated. When the temperature of the enclosure exceeded the setpoint temperature, the TED8040 controllers reversed the direction of the current, so that it flowed in the direction of the blue arrows. Under this condition, the circuit diverted the current from the heaters and the chamber was allowed to cool.

Experimental Results

The data curves plotted in Figure 5 are the dark currents measured for the Si-based FDS1010, the Ge-based FDG50, the GaP-based FGAP71, and the InGaAs-based FGA10. Data were acquired continuously while the temperature was between 25 °C and 55 °C (shaded region of Figure 6). Figure 6 is representative of the temperature measured at the photodiode during the experiment. The temperature profile included an initial segment of increasing temperature, followed by a soak that allowed the photodiode to reach the maximum temperature, and concluded with a cool-down. The data plotted in Figure 5 include all dark current measurements measured between 25 °C and 55 °C; current measurements taken at the same temperature, but at different times, overlay one another for each diode.

The data curves plotted in Figure 5 show that the measured dark current magnitudes differed depending on the material composing the photodiode. From lowest to highest:

- GaP-Based Detector FGAP71 (Lowest Dark Current)
- InGaAs-Based Detector FGA10
- Si-Based Detector FDS1010
- Ge-Based Detector FDG50 (Highest Dark Current)

These span approximately 6 orders of magnitude. In all cases, the dark current increased with the temperature of the photodiode, as expected. The individual points on this graph, plotted as diamonds, are the values of the dark current specified for each detector at 25 °C. These points specify a maximum value of

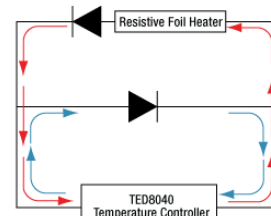
Figure 2: The Nested Metal Box Test Fixture with Covers Removed and FGA10 Installed

Black insulating foam lines the interiors of both boxes.
A: Thermistor; B: FGA10; C: BNC-to-BNC Feedthrough; D: Outer Box; E: Inner Box; F: BNC-to-Triax Feedthrough; G: BNC-to-BNC Feedthrough



Click to Enlarge

Figure 3: The Test Setup
The custom-built temperature chamber is on the top of the cart, and the temperature control instrumentation that includes the PRO8000 and TED8040 cards is on the cart's lower shelf.



Click to Enlarge

Figure 4: An electrical circuit that included a resistive foil heater, TED8040 temperature controller, and two rectifying diodes controlled current flow through the resistive current heater as described in the text.

dark current at 25 °C; each diode's dark current must be equal to or less than this value at 25 °C, but the dark current may exceed this specification at higher temperatures, as is the case for all but the measured FDS1010 detector.

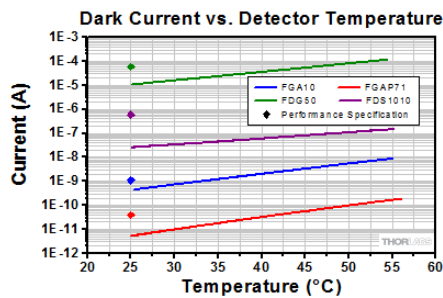


Figure 5: Dark Current Data Measured for Four Unmounted Photodiodes

The discrete data points, plotted as diamonds, are values of the dark current specified for each detector at 25 °C.

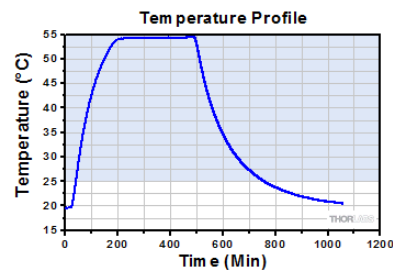


Figure 6: Temperature of a Representative Photodiode Controlled by the Conditions in the Environmental Chamber

Dark current measurements were acquired between 25 °C and 55 °C (indicated by the shaded region) and are plotted in Figure 5 .

Experimental Limitations

Measurements were performed using a single representative of each detector type, as these data were intended to illustrate overall trends. These data should not be taken as specific for a particular diode. The measured dark current is a function of voltage bias, temperature dependence of resistive loads, and other effects. Efforts were made to suppress their influence on these measurements, including using the Keithly 6487 ammeter to provide the required 5 V reverse bias. Using the ammeter removed the need to use a load resistor, which may exhibit its own temperature dependence. The thermistor was placed as close to the semiconductor sensor as was possible, but it was not placed in direct contact with the sensor. Because of this, there may have been a difference between the measured temperature and the temperature of the semiconductor material. The dark current was measured while the temperature of the environmental chamber was continuously varied. Humidity was not controlled during this experiment.

[1] J. Liu, Photonic Devices. Cambridge University Press, Cambridge, UK, 2005

[Hide NEP](#)

NEP

Noise Equivalent Power (NEP) as a Function of Temperature

Noise Equivalent Power (NEP) was determined as a function of temperature for several unmounted photodetectors. As is described in the following section, NEP is a common metric used to describe the minimum sensitivity of a photodetector. Measurements were taken for silicon (Si), germanium (Ge), gallium phosphide (GaP), and indium gallium arsenide (InGaAs) reverse-biased photodiodes over temperatures from 25 °C to approximately 55 °C.

Noise Equivalent Power

The most general definition of NEP is "the input signal power that results in a signal-to-noise ratio (SNR) of 1 in a 1 Hz output bandwidth." [1] Therefore, in order to determine the NEP, the minimum noise of the photodiode must be determined. When the optical signal is blocked, noise is still present, which is generated by the detector itself. There are two main contributors to photodiode noise: the shot noise due to dark current and thermal noise due to the shunt resistance.

Dark current is a relatively small electric current present in photosensitive devices that flows through the device, including when there is no incident light. More information on the dark current can be found in the "Dark Current as a Function of Temperature" section above. Shot noise is due to the quantized nature of the charge carriers. For the case where there is no light incident on the detector, it can be calculated from the dark current of the detector using the equation [2]

$$i_s = \sqrt{2qI_D f_{BW}}$$

where i_s is the shot noise, I_D is the dark current, q is the electron charge, and f_{BW} is the bandwidth, which will be set to 1 Hz to allow for comparison between different photodiodes.

Thermal, or Johnson, noise is due to the random thermal motion of the charge carriers. Thermal noise will be generated only by the resistive elements of the system. For the photodiode detector, the shunt resistance needs to be considered. Shunt resistance is the resistance of the zero-biased photodiode p-n junction; put another way, it is the inverse of the slope of the I-V curve at the zero-voltage point. Since it is difficult to correctly calculate the slope at the zero crossing, the generally accepted industry practice is to measure the current at $V = \pm 10$ mV and then calculate the slope. Then the thermal noise due to the shunt resistance, R_{SH} , can be expressed as:

$$i_T = \sqrt{\frac{4k_B T}{R_{SH}} f_{BW}}$$

where i_T is the thermal noise (expressed as a current), k_B is Boltzmann's constant, T is temperature, R_{SH} is shunt resistance, and f_{BW} is the bandwidth.

The total noise, i_{total} , is the quadrature sum of all noise sources:

$$i_{total} = \sqrt{i_S^2 + i_T^2}$$

Note that this result is the total noise expressed for the current output of the photodiode, while the NEP is expressed in terms of incident optical power. Thus, to compare with the NEP specifications a typical responsivity value, \mathfrak{R} , is chosen for the specified wavelength:

$$NEP = \frac{i_{total}}{\mathfrak{R}}$$

Also, to allow for comparison between different diodes, we set the bandwidth to 1 Hz for the calculation.

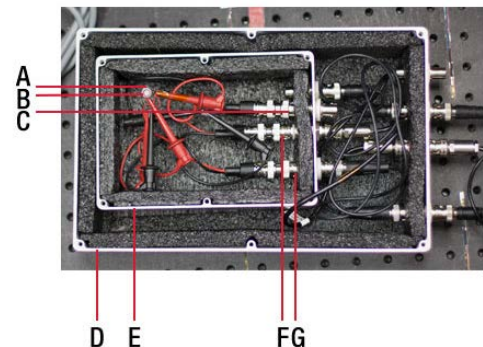
Experiment: Dark Current and Shunt Resistance Measurements

NEP was determined over 25 to 55 °C for four representative unpackaged photodiodes: the Si-based FDS1010, the Ge-based FDG50, the GaP-based FGAP71, and the InGaAs-based FGA10.

Experimental Setup

The experimental setup was designed to ensure a constant reverse-bias voltage across the photodiode, control the temperature of the detector, block light from reaching the detector, and establish an electrical path between the detector and the Keithley 6487 ammeter that isolated the measured current from extraneous electromagnetic interference (EMI) noise sources. Dark currents for these detectors can be on the order of nA, which made it important to control these conditions to ensure accurate measurements.

The detector enclosure consisted of a pair of nested aluminum metal boxes, which are shown with their covers off in Figure 1. Only one box would be required to create a light-tight environment for the photodiode, but an outer box was included in the setup to shield the inner box from EMI. The detector was placed inside the inner box, and it was electrically connected to the Keithley 6487 ammeter. The ammeter provided the required reverse-bias voltage and received the output current signal. The electrical signals between the ammeter and the photodiode were routed through the two boxes using a combination of cables and feedthroughs. The bias voltage was connected to the photodiode using coax cables and BNC-to-BNC feedthroughs in the walls of both metal boxes. The current signal from the photodiode was connected to the BNC end of a BNC-to-Triax feedthrough



Click to Enlarge
Figure 1: The nested metal box test fixture with covers removed and FGA10 installed.
 Black insulating foam lines the interiors of both boxes.
 A: Thermistor; B: FGA10; C: BNC-to-BNC Feedthrough; D: Outer Box;
 E: Inner Box; F: BNC-to-Triax Feedthrough; G: BNC-to-BNC Feedthrough

integrated into the wall of the inner box. The signal was then routed through the outer box and to the Keithley 6487 using triax cables and a Triax-to-Triax feedthrough in the outer box. Triax cables were used because coax cables are poorly shielded, and using a coax cable to route the signal to the ammeter could introduce noise from EMI sources to the signal read from the detector. As the outer box shields the inner box from EMI, the noise introduced on the signal as it travels from the detector to the BNC-to-Triax feedthrough is mitigated.

For dark current measurements, the bias voltage was set to 5 V. In order to calculate the shunt resistance, measurements of the current were made with the bias voltage set to +10 mV and -10 mV.

Thermistors were used to monitor the temperatures of each photodiode continuously during the experiment. A piece of thermal tape was used to hold the thermistor flush against the TO cans of the FDG50, FGAP71, and the FGA10 during testing. The photosensor of the FDS1010 is mounted on a ceramic substrate, and when it was tested the thermistor was taped to the back of the substrate. The electrical connection between the thermistor and TSP01 temperature logger was performed using BNC cables, BNC-to-BNC bulkhead feedthroughs to route the signal out of the nested boxes, and a custom BNC-to-phono jack cable to connect to the temperature logger.

A custom temperature chamber based on a XE25C9 standard enclosure was used to conduct these tests. It is shown on top of the cart in Figure 3. The enclosure had a floor and four walls, and insulation was attached to all inner and outer surfaces. A lid for the enclosure was fashioned from a sheet of hardboard bordered with XE25 rails, and insulation was attached to the inner surface of the hardboard. Six resistive foil heaters were affixed to the walls of the XE25C9 enclosure, and they were driven using the PRO8000 chassis fitted with six TED8040 thermoelectric cooler (TEC) controller cards placed on the bottom shelf of the cart in Figure 2. Each TED8040 was interfaced with a heater and a thermistor installed in the chamber. The reading from the thermistor determined the current sent to drive the heater. The chamber was not actively cooled; cooling was instead performed by withdrawing the current driving the heaters and, as an option, opening the lid of the chamber.

The TED8040 units are designed to be interfaced with TECs, which produce heat when current flows in one direction, and which provide cooling when the current flows in the opposite direction. Because of this, when the enclosure exceeded the setpoint temperature, the TED8040 units in this experimental setup did not cut off the driving current. They instead reversed the current flow in an effort to produce cooling. In contrast to TECs, resistive foil heaters generate heat regardless of the direction of current flowing through them. In order to divert the driving current from the heaters, an electrical circuit, diagrammed in Figure 3, that included two rectifying diodes was designed and implemented. Rectifying diodes allow current to flow only in one direction. When the temperature reading from the thermistor was lower than the setpoint temperature, current flowed in the direction of the red arrows and through the resistive heater, and heat was generated. When the temperature of the enclosure exceeded the setpoint temperature, the TED8040 controllers reversed the direction of the current, so that it flowed in the direction of the blue arrows. Under this condition, the circuit diverted the current from the heaters and the chamber was allowed to cool.

Experimental Results

The data curves plotted in Figure 4 are the dark currents measured for the Si-based FDS1010, the Ge-based FDG50, the GaP-based FGAP71, and the InGaAs-based FGA10. Figure 5 shows the calculated shunt resistance values for the same diodes as Figure 4. Data were acquired continuously while the temperature was between 25 °C and 55 °C (shaded region of Figure 7). Figure 7 is representative of the temperature measured at the photodiode during the experiment. The temperature profile included an initial segment of increasing temperature, followed by a soak that allowed the photodiode to reach the maximum temperature, and concluded with a cool-down. The data plotted in Figures 4 and 5 include all dark current measurements measured between approximately 25 °C and 55 °C; current measurements taken at the same temperature, but at different times, overlay one another for each diode.

As shown in Figure 5, the shunt resistance for the measured GaP, InGaAs, and Si detectors is relatively large; therefore in many situations it can be ignored. For the Ge-based FDG50 the shunt resistance is relatively low, especially at higher temperatures. For this diode the shunt resistance might need to be considered if there is a high load involved.

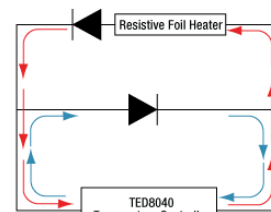
Figure 6 shows the calculated NEP vs. temperature for each diode. Since the NEP is a function of responsivity, which varies with wavelength, the NEP values are calculated at the peak responsivity value as given in the table to the right.

The data curves plotted in Figure 6 show that the calculated NEP magnitudes differed depending on the material composing the photodiode. From lowest to highest:

- GaP-Based Detector FGAP71 (Lowest NEP)



Click to Enlarge
Figure 2: The Test Setup
 The custom-built temperature chamber is on the top of the cart, and the temperature control instrumentation that includes the PRO8000 and TED8040 cards is on the cart's lower shelf.



Click to Enlarge
Figure 3: An electrical circuit that included a resistive foil heater, TED8040 temperature controller, and two rectifying diodes controlled current flow through the resistive current heater as described in the text.

Responsivity Used for NEP Calculation	
FGA10	1.05 A/W @ 1550 nm

- InGaAs-Based Detector FGA10
- Si-Based Detector FDS1010
- Ge-Based Detector FDG50 (Highest NEP)

FDG50	0.85 A/W @ 1550 nm
FGAP71	0.12 A/W @ 440 nm
FDS1010	0.725 A/W @ 970 nm

These span approximately 6 orders of magnitude. In all cases, the dark current increased with the temperature of the photodiode, as expected. The individual points on this graph, plotted as diamonds, are the values of the dark current specified for each detector at 25 °C. These points specify a maximum value of dark current at 25 °C; each diode's dark current and NEP must be equal to or less than this value at 25 °C, but the dark current and NEP may exceed this specification at higher temperatures.

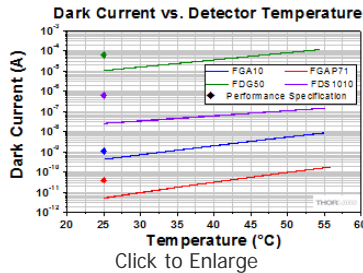


Figure 4: Dark Current Data Measured for Four Unmounted Photodiodes
The discrete data points, plotted as diamonds, are values of the dark current specified for each detector at 25 °C.

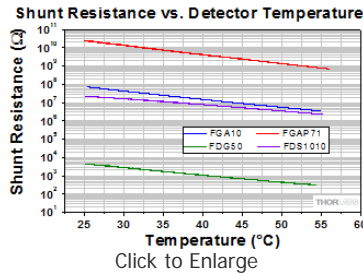


Figure 5: Shunt Resistance Calculated as Described in the Text for Four Unmounted Photodiodes

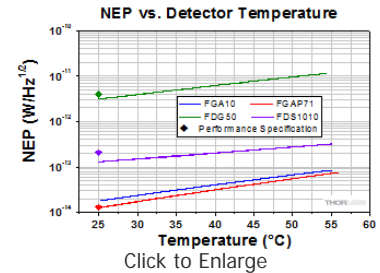


Figure 6: NEP Calculated from the Quadrature Sum of Shot Noise and Thermal Noise for Four Unmounted Photodiodes
The discrete data points, plotted as diamonds, are values of the NEP specified for each detector at 25 °C. There is no point for FGA10 since the NEP is not specified at the peak responsivity wavelength.

Experimental Limitations

Measurements were performed using a single representative of each detector type, as these data were intended to illustrate overall trends. These data should not be taken as specific for a particular diode. The measured currents were functions of voltage bias, temperature dependence of resistive loads, and other effects. Efforts were made to suppress their influence on these measurements, including using the Keithley 6487 ammeter to provide the required 5 V reverse bias. Using the ammeter removed the need to use a load resistor, which may exhibit its own temperature dependence. The thermistor was placed as close to the semiconductor sensor as was possible, but it was not placed in direct contact with the sensor. Because of this, there may have been a difference between the measured temperature and the temperature of the semiconductor material. The currents were measured while the temperature of the environmental chamber was continuously varied. Humidity was not controlled during this experiment.

[1] Thorlabs' Noise Equivalent Power White Paper.

[2] Quimby, Richard S. Photonics and Lasers: An Introduction. Wiley-Interscience, Hoboken, NJ, 2006, pp 241-244.

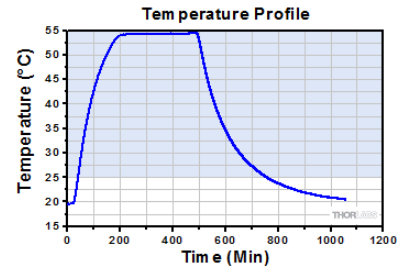


Figure 7: Temperature of a Representative Photodiode Controlled by the Conditions in the Environmental Chamber
Dark current measurements were acquired between 25 °C and 55 °C (indicated by the shaded region) and are plotted in Figure 5 .

Hide Beam Size

BEAM SIZE

We present laboratory measurements showing the effect of beam size on the saturation point of a Thorlabs silicon photodiode. As defined here, saturation is a 1% deviation from the linear response region. As illustrated in Figure 1, the photodiode saturated at lower incident power levels as the beam size decreased. Several additional calculations and experiments were performed to verify the cause of the change in saturation was not a function of the power density. These results suggest that users should be cognizant of the beam size when attempting to measure absolute power with a power sensor, such as our S130C photodiode power sensor.

For our experiment, we used the SM1PD1A mounted photodiode, which consists of an FDS1010 photodiode in an SM1-threaded housing. An 830 nm superluminescent diode was used as the light source. A beamsplitter directed 20% of the light to a monitor photodiode while the remainder was transmitted through a focusing lens. Power values were calibrated using an integrating sphere, while the beam size of the focusing beam was calibrated with a beam profiler mounted to a translation stage. After calibration, the beam profiler was replaced with the device under test (DUT), an SM1PD1A at a 0 V bias. The output current was measured with an ammeter to remove the need for a load resistor. We then recorded datasets as the beam diameter was continuously scanned from 0.06 mm to 5 mm while power was held constant, as well as measurements for

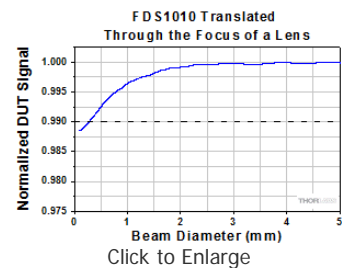


Figure 1: Normalized change in output current for a fixed incident power as the photodiode Device Under Test (DUT), FDS1010, was translated through the focus of a lens.

beam diameters ranging from 1 mm to 5 mm (measured to the 5% clip level) as the incident power was continuously scanned from 0.12 mW to 5 mW.

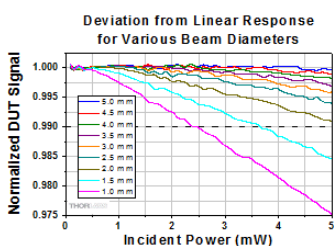
The figures show the results from the measurements. Figure 1 (right) and Figure 2 (below) show the deviation from linear response for continuously varying beam diameter at a fixed 1 mW incident power (Figure 1) and continuously varying incident power for several beam diameters (Figure 2). Figure 1 shows that for a 1 mW input, the photodiode saturated at beam sizes less than 300 μm . Figure 2 shows that beam diameters ≥ 2 mm did not saturate at the power levels investigated.

Lab Facts

Click for Full Lab Facts Summary

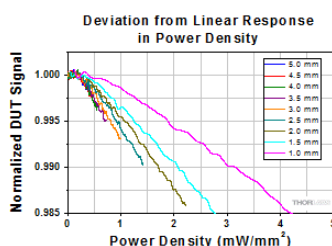
One hypothesis for these results was that local saturation due to a large power density locally depleted or reduced the population of available carriers. In Figure 3, we calculated the power density by taking the quotient of the measured power and beam diameter presented in Figure 2 and plotted the current output as a function of that power density. If the results were due to local saturation, we would have expected that all of the beam diameters would saturate at a single power density; however, this was not the case.

Since the results presented in Figure 3 coupled the beam size change with a change in optical power density, we performed another experiment to increase the power density incident on the sensor within the same envelope of beam area to see if there was a change in the saturation point. This was done by segmenting the Gaussian beam into an array of beamlets with a microlens array, concentrating the overall optical power into smaller spots within the same Gaussian envelope. This created larger power densities while maintaining a similar electrical path to the sensor leads. Figure 4 shows the same results as Figure 2 with the results from the microlens array overlaid as dashed lines. Since the results are nearly identical to the original Gaussian beam for all diameters, the saturation appears to be dependent on the overall beam diameter and independent of the power density. In the complete Lab Facts presentation, we discuss how these results support the theory of Scholze *et al.* that the change in saturation with beam size is due to a change in the series resistance of the photodiode [1].



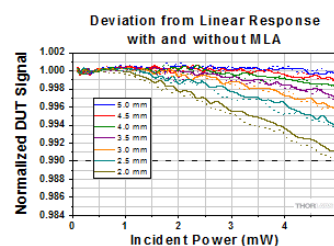
Click to Enlarge

Figure 2: Percent Deviation from the linear response with increasing power for 1 mm - 5 mm beam diameters. The 1% deviation level is indicated with a dashed horizontal line.



Click to Enlarge

Figure 3: Normalized output current versus power density for 1 mm - 5 mm beam diameters. This shows the saturation effects do not appear to be based on a single power density.



Click to Enlarge

Figure 4: Normalized output current versus optical power for 2 mm - 5 mm beam diameter with (Dashed Line) and without (Solid Line) the microlens array (MLA) prior to the photodiode.

[1] F. Scholze, R. Klein, R. Muller, Linearity of silicon photodiodes for EUV radiation. 2004 Proc. SPIE 5374 926–34.

[Hide Bias Voltage](#)

BIAS VOLTAGE

The Effects of Incident Optical Power on the Effective Reverse Bias Voltage of Photodiodes

Introduction

The bandwidth (and rise time) of a photodiode is known to be a function of the effective bias across it. Therefore, the effective bias must be tuned in response to the generated photocurrent from the optical power incident on the diode to maintain the desired bandwidth. This lab fact investigates the relationship between the effective reverse bias voltage across a photodiode and the CW optical power incident on it in order to create a reliable model of a biased photodiode.

Lab Facts

Click for Full Lab Facts Summary

Circuit Analysis

To begin creating this model, the photodiode circuit shown in Figure 2 to the right is examined using Ohm's law and assuming a constant DC voltage source; this yields the equation

$$V_{\text{eff}} = V_0 - i_{\text{PD}} * (R_{\text{P}} + R_{\text{L}}). \quad (1)$$

The effective bias voltage (V_{eff}) across the photodiode equals the initial voltage from the source (V_0) minus the product of the photocurrent (i_{PD}) and the sum of the resistance of the bias module's resistor (R_{P}) and the load resistor (R_{L}).

To find how V_{eff} changes with respect to the incident optical power (P), i_{PD} is replaced in the above equation with its definition as the product of the wavelength-dependent responsivity [$\mathfrak{R}(\lambda)$] of the photodiode and P :

$$i_{\text{PD}} = \mathfrak{R}(\lambda) * P. \quad (2)$$

Using Ohm's law on the load resistor such that $i_{\text{PD}} = V_L / R_L$, the equation above was rewritten to solve for $\mathfrak{R}(\lambda)$:

$$\mathfrak{R}(\lambda) = V_L / (P * R_L). \quad (3)$$

Assuming that the voltage drop across the load resistor (V_L) is linear with respect to increasing P , the ratio of the change in V_L and P can be established as the ratio:

$$m = \Delta V_L / \Delta P. \quad (4)$$

These equations can be combined to form:

$$V_{\text{eff}} = V_0 - (m / R_L) * P * (R_P + R_L). \quad (5)$$

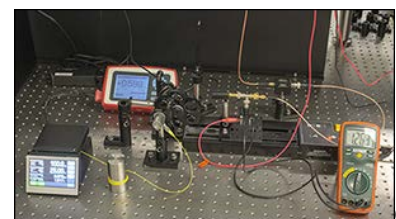
The ratio m can be calculated from empirical measurements of V_L and P for each photodiode, allowing this equation to be used as a model for how V_{eff} changes with respect to P .

Experiment

An experiment was developed to measure the change in V_L with respect to changes in P . Output from a fiber-coupled laser diode was collimated, passed through a neutral density filter, and then focused onto the Device Under Test (DUT) via an off-axis parabolic mirror. A photograph of the setup used can be seen in Figure 1 to the upper right. Neutral density filters with a range of optical densities were used to vary the power incident on the photodiode. For each photodiode used, the distance between the sensor surface and focusing mirror was adjusted so that the spot size was approximately half the size of each photodiodes' detector area. An oscilloscope was used to measure V_0 , V_L , and the sum $V_{\text{eff}} + V_L$. A multimeter was used to measure the effective bias directly.

Results

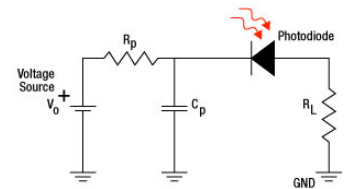
V_L was plotted against P for each DUT; an example of the results for the silicon photodiode can be seen in Figure 3 to the right. A linear trend line was created for each data set, and the slope of that line corresponds to m in Equation 4. This value can be used in Equation 5 to calculate the effective bias voltage. Then, V_{eff} can be plotted with respect to the incident power and compared to the measured values from the oscilloscope. These results are shown in the three graphs displayed in Figure 4 below. The model was found to be consistent with measured experimental results, which showed that V_{eff} decreases as P increases (with V_0 , R_P , and R_L held constant). This effect is significant, because the voltage set at the voltage source is not necessarily the bias voltage applied to the photodiode; one must account for resistive components within the circuit to calculate the effective bias voltage applied across the photodiode.



Click to

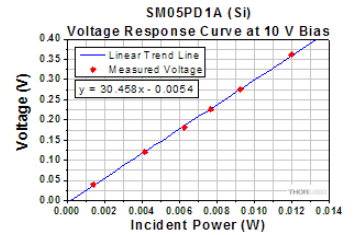
Enlarge

Figure 1 : This setup was used in the experiment in order to verify our model of the effective voltage across the photodiode.



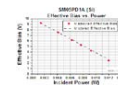
[Click to Enlarge](#)

Figure 2 : Circuit Diagram of Biased Photodiode

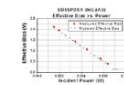


[Click to Enlarge](#)

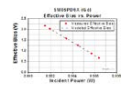
Figure 3 : A single voltage vs. incident power graph used to find m for the final model, Equation 5.



[Click to Enlarge](#)



[Click to Enlarge](#)



[Click to Enlarge](#)

Figure 4 :

Measured Effective Bias Values for Various Photodiodes Plotted with their Modeled Values

[Hide Pulse Calculations](#)

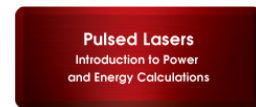
PULSE CALCULATIONS

Pulsed Laser Emission: Power and Energy Calculations

Determining whether emission from a pulsed laser is compatible with a device or application can require referencing parameters that are not supplied by the laser's manufacturer. When this is the case, the necessary parameters can typically be calculated from the available information. Calculating peak pulse power, average power, pulse energy, and related parameters can be necessary to achieve desired outcomes including:

- Protecting biological samples from harm.
- Measuring the pulsed laser emission without damaging photodetectors and other sensors.
- Exciting fluorescence and non-linear effects in materials.

Pulsed laser radiation parameters are illustrated in Figure 1 and described in the table. For quick reference, a list of equations are provided below. The document available for download provides this information, as well as an introduction to pulsed laser emission, an overview of relationships among the different parameters, and guidance for applying the calculations.



Click above to download the full report.

Equations:

Period and repetition rate are reciprocal: $\Delta t = \frac{1}{f_{rep}}$ and $f_{rep} = \frac{1}{\Delta t}$

Pulse energy calculated from average power: $E = \frac{P_{avg}}{f_{rep}} = P_{avg} \cdot \Delta t$

Average power calculated from pulse energy: $P_{avg} = \frac{E}{\Delta t} = E \cdot f_{rep}$

Peak pulse power estimated from pulse energy: $P_{peak} \approx \frac{E}{\tau}$

Peak power and average power calculated from each other:

$$P_{peak} = \frac{P_{avg}}{f_{rep} \cdot \tau} = \frac{P_{avg} \cdot \Delta t}{\tau} \quad \text{and} \quad P_{avg} = P_{peak} \cdot f_{rep} \cdot \tau = \frac{P_{peak} \cdot \tau}{\Delta t}$$

Peak power calculated from average power and duty cycle:*

$$P_{peak} = \frac{P_{avg}}{\tau / \Delta t} = \frac{P_{avg}}{\text{duty cycle}}$$

*Duty cycle ($\tau / \Delta t$) is the fraction of time during which there is laser pulse emission.

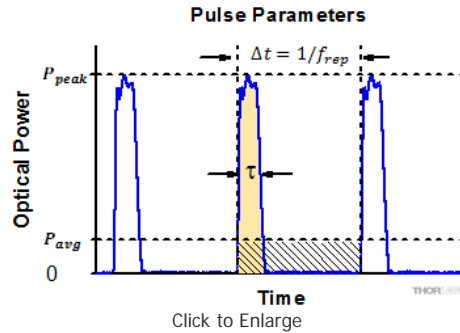


Figure 1: Parameters used to describe pulsed laser emission are indicated in the plot (above) and described in the table (below). **Pulse energy (E)** is the shaded area under the pulse curve. Pulse energy is, equivalently, the area of the diagonally hashed region.

Parameter	Symbol	Units	Description
Pulse Energy	E	Joules [J]	A measure of one pulse's total emission, which is the only light emitted by the laser over the entire period. The pulse energy equals the shaded area, which is equivalent to the area covered by diagonal hash marks.
Period	Δt	Seconds [s]	The amount of time between the start of one pulse and the start of the next.
Average Power	P_{avg}	Watts [W]	The height on the optical power axis, if the energy emitted by the pulse were uniformly spread over the entire period.
Instantaneous Power	P	Watts [W]	The optical power at a single, specific point in time.
Peak Power	P_{peak}	Watts [W]	The maximum instantaneous optical power output by the laser.
Pulse Width	τ	Seconds [s]	A measure of the time between the beginning and end of the pulse, typically based on the full width half maximum (FWHM) of the pulse shape. Also called pulse duration .
Repetition Rate	f_{rep}	Hertz [Hz]	The frequency with which pulses are emitted. Equal to the reciprocal of the period.

Example Calculation:

Is it safe to use a detector with a specified maximum peak optical input power of **75 mW** to measure the following pulsed laser emission?

- Average Power: 1 mW
- Repetition Rate: 85 MHz
- Pulse Width: 10 fs

The energy per pulse:

$$E = \frac{P_{avg}}{f_{rep}} = \frac{1 \text{ mW}}{85 \text{ MHz}} = \frac{1 \times 10^{-3} \text{ W}}{85 \times 10^6 \text{ Hz}} = 1.18 \times 10^{-11} \text{ J} = 11.8 \text{ pJ}$$

seems low, but the peak pulse power is:

$$P_{peak} = \frac{P_{avg}}{f_{rep} \cdot \tau} = \frac{1 \text{ mW}}{85 \text{ MHz} \cdot 10 \text{ fs}} = 1.18 \times 10^3 \text{ W} = \mathbf{1.18 \text{ kW}}$$

It is **not safe** to use the detector to measure this pulsed laser emission, since the peak power of the pulses is >5 orders of magnitude higher than the detector's maximum peak optical input power.

CROSS REFERENCE

The following table lists Thorlabs' selection of photodiodes and photoconductive detectors. Item numbers in the same row contain the same detector element.

Photodetector Cross Reference						
Wavelength	Material	Unmounted Photodiode	Unmounted Photoconductor	Mounted Photodiode	Biased Detector	Amplified Detector
150 - 550 nm	GaP	FGAP71	-	SM05PD7A	DET25K2	PDA25K2
200 - 1100 nm	Si	FDS010	-	SM05PD2A SM05PD2B	DET10A2	PDA10A2
	Si	-	-	SM1PD2A	-	-
320 - 1000 nm	Si	-	-	-	-	PDA8A2
320 - 1100 nm	Si	FD11A	-	SM05PD3A	-	PDF10A2
	Si	-	-	-	DET100A2	PDA100A2
340 - 1100 nm	Si	FDS10X10	-	-	-	-
350 - 1100 nm	Si	FDS100 FDS100-CAL ^a	-	SM05PD1A SM05PD1B	DET36A2	PDA36A2
	Si	FDS1010 FDS1010-CAL ^a	-	SM1PD1A SM1PD1B	-	-
400 - 1000 nm	Si	-	-	-	-	PDA015A(/M) FPD310-FS-VIS FPD310-FC-VIS FPD510-FC-VIS FPD510-FS-VIS FPD610-FC-VIS FPD610-FS-VIS
400 - 1100 nm	Si	FDS015 ^b	-	-	-	-
	Si	FDS025 ^b FDS02 ^c	-	-	DET02AFC(/M) DET025AFC(/M) DET025A(/M) DET025AL(/M)	-
400 - 1700 nm	Si & InGaAs	DSD2	-	-	-	-
500 - 1700 nm	InGaAs	-	-	-	DET10N2	-
750 - 1650 nm	InGaAs	-	-	-	-	PDA8GS
800 - 1700 nm	InGaAs	FGA015	-	-	-	PDA015C(/M)
	InGaAs	FGA21 FGA21-CAL ^a	-	SM05PD5A	DET20C2	PDA20C2 PDA20CS2
	InGaAs	FGA01 ^b FGA01FC ^c	-	-	DET01CFC(/M)	-
	InGaAs	FDGA05 ^b	-	-	-	PDA05CF2
	InGaAs	-	-	-	DET08CFC(/M) DET08C(/M) DET08CL(/M)	PDF10C/M
800 - 1800 nm	Ge	FDG03 FDG03-CAL ^a	-	SM05PD6A	DET30B2	PDA30B2
	Ge	FDG50	-	-	DET50B2	PDA50B2
	Ge	FDG05	-	-	-	-

900 - 1700 nm	InGaAs	FGA10	-	SM05PD4A	DET10C2	PDA10CS2
900 - 2600 nm	InGaAs	FD05D	-	-	DET05D2	-
		FD10D	-	-	DET10D2	PDA10D2
950 - 1650 nm	InGaAs	-	-	-	-	FPD310-FC-NIR FPD310-FS-NIR FPD510-FC-NIR FPD510-FS-NIR FPD610-FC-NIR FPD610-FS-NIR
1.0 - 5.8 μ m	InAsSb	-	-	-	-	PDA10PT(-EC)
2.0 - 5.4 μ m	HgCdTe (MCT)	-	-	-	-	PDA10JT(-EC)
2.0 - 8.0 μ m	HgCdTe (MCT)	VML8T0 VML8T4 ^d	-	-	-	PDAVJ8
2.0 - 10.6 μ m	HgCdTe (MCT)	VML10T0 VML10T4 ^d	-	-	-	PDAVJ10
2.7 - 5.0 μ m	HgCdTe (MCT)	VL5T0	-	-	-	PDAVJ5
2.7 - 5.3 μ m	InAsSb	-	-	-	-	PDA07P2

- ^aCalibrated Unmounted Photodiode
- ^bUnmounted TO-46 Can Photodiode
- ^cUnmounted TO-46 Can Photodiode with FC/PC Bulkhead
- ^dPhotovoltaic Detector with Thermoelectric Cooler

Hide GaP Photodiode - UV Wavelengths

GaP Photodiode - UV Wavelengths

- ▶ Detection of Extremely Short Wavelengths (150 - 550 nm)
- ▶ Mounted in a Hermetically Sealed Package with a Sapphire Window

Item #	Info	Wavelength Range	Active Area	Package	Rise/Fall Time ^a	NEP (W/Hz ^{1/2})	Dark Current	Junction Capacitance	Compatible Sockets
FGAP71		150 - 550 nm	4.8 mm ² (2.2 mm x 2.2 mm)	TO-39	55 ns / 55 ns @ 405 nm, 5 V	1.3 x 10 ⁻¹⁴ @ 440 nm, 5 V	15 pA (Typ.) 40 pA (Max) @ 5 V	1000 pF (Typ.) @ 0 V	STO5S STO5P

- ^aTypical Values; R_L = 50 Ω

Part Number	Description	Price	Availability
FGAP71	GaP Photodiode, 55 ns Rise Time, 150-550 nm, 2.2 mm x 2.2 mm Active Area	\$97.93	5-8 Days

Hide Si Photodiodes - VIS Wavelengths

Si Photodiodes - VIS Wavelengths

Click Image for Details								
Item #	FDS010	FD11A	FDS10X10	FDS100	FDS1010	FDS015	FDS02	FDS025
Key Feature	High Speed, UV Grade Fused Silica Window to Provide Sensitivity Down to 200 nm	Lowest Dark Current in TO-18 Can with a Window	Low Dark Current in 10 mm x 10 mm Ceramic Package	High Speed, Largest Sensor in a TO-5 Can	High Speed, Large Active Area and Mounted on an Insulating Ceramic Substrate	Highest Speed and Lowest Capacitance in a TO-46 Can with an AR-Coated Window	High Speed and Low Capacitance in a Direct Fiber-Coupled FC/PC Package	High Speed and Low Capacitance in a TO-46 Can with a Ball Lens
Info								
Wavelength	^a 320 - 1100 nm	320 - 1100 nm	340 - 1100 nm	350 - 1100 nm	350 - 1100 nm	400 - 1100 nm	400 - 1100 nm	400 - 1100 nm

Range	200 - 1100 nm							
Active Area	0.8 mm ² (Ø1.0 mm)	1.21 mm ² (1.1 mm x 1.1 mm)	100 mm ² (10 mm x 10 mm)	13 mm ² (3.6 mm x 3.6 mm)	100 mm ² (10 mm x 10 mm)	0.018 mm ² (Ø150 µm)	0.049 mm ² (Ø0.25 mm)	0.049 mm ² (Ø0.25 mm)
Rise/Fall Time ^b	1 ns / 1 ns @ 830 nm, 10 V	400 nsc,d @ 650 nm, 0 V	150 ns / 150 ns ^d @ 5 V	10 ns / 10 ns ^d @ 632 nm, 20 V	65 ns / 65 ns ^d @ 632 nm, 5 V	35 ps / 200 ps @ 850 nm, 5 V	47 ps / 246 ps @ 850 nm, 5 V	47 ps / 246 ps @ 850 nm, 5 V
NEP (W/Hz ^{1/2})	5.0 x 10 ⁻¹⁴ @ 830 nm, 10 V	6.8 x 10 ⁻¹⁶ @ 960 nm, 0 V	1.50 x 10 ⁻¹⁴ @ 960 nm	1.2 x 10 ⁻¹⁴ @ 900 nm, 20 V	2.07 x 10 ⁻¹³ @ 970 nm, 5 V	8.60 x 10 ⁻¹⁵ @ 850 nm, 5 V	9.29 x 10 ⁻¹⁵ @ 850 nm, 5 V	9.29 x 10 ⁻¹⁵ @ 850 nm, 5 V
Dark Current	0.3 nA (Typ.) @ 10 V	2.0 pA (Max) @ 10 mV	200 pA @ 5 V	1.0 nA (Typ.) @ 20 V	600 nA (Max) @ 5 V	0.03 nA (Typ.) @ 5 V	35 pA (Typ.) @ 5 V	35 pA (Typ.) @ 5 V
Junction Capacitance	6 pF (Typ.) @ 10 V	140 pF (Typ.) @ 0 V	380 pF @ 5 V	24 pF (Typ.) @ 20 V	375 pF (Typ.) @ 5 V	0.65 pF (Typ.) @ 5 V	0.94 pF (Typ.) @ 5 V	0.94 pF (Typ.) @ 5 V
Package	TO-5	TO-18	Ceramic	TO-5	Ceramic	TO-46	TO-46, FC/PC Bulkhead	TO-46
Compatible Sockets	STO5S STO5P	STO46S STO46P	Not Available	STO5S STO5P	Not Available	STO46S STO46P	STO46S STO46P	STO46S STO46P

- ~~Δ~~When long-term UV light is applied, the product specifications may degrade. For example, the product's UV response may decrease and the dark current may increase. The degree to which the specifications may degrade is based upon factors such as the irradiation level, intensity, and usage time.
- ~~Δ~~Typical Values; R_L = 50 Ω Unless Otherwise Specified
- ~~Δ~~Measured with a 1 kΩ Resistor
- ~~Δ~~The photodiode will be slower at NIR wavelengths.

Part Number	Description	Price	Availability
FDS010	Si Photodiode, 1 ns Rise Time, 200 - 1100 nm, Ø1 mm Active Area	\$48.15	Today
FD11A	Si Photodiode, 400 ns Rise Time, 320 - 1100 nm, 1.1 mm x 1.1 mm Active Area	\$14.58	Today
FDS10X10	Si Photodiode, 150 ns Rise Time, 340 - 1100 nm, 10 mm x 10 mm Active Area	\$114.70	Today
FDS100	Si Photodiode, 10 ns Rise Time, 350 - 1100 nm, 3.6 mm x 3.6 mm Active Area	\$14.94	Today
FDS1010	Si Photodiode, 65 ns Rise Time, 350 - 1100 nm, 10 mm x 10 mm Active Area	\$55.73	Today
FDS015	Si Photodiode, 35 ps Rise Time, 400 - 1100 nm, Ø150 µm Active Area	\$53.05	Today
FDS02	Si Photodiode, 47 ps Rise Time, 400 - 1100 nm, Ø0.25 mm Active Area, FC/PC Bulkhead	\$83.59	Today
FDS025	Si Photodiode, 47 ps Rise Time, 400 - 1100 nm, Ø0.25 mm Active Area	\$34.36	Today

[Hide InGaAs Photodiodes - NIR Wavelengths](#)

InGaAs Photodiodes - NIR Wavelengths

Click Image for Details								
Item #	FGA01	FGA01FC	FGA015	FDGA05	FGA21	FGA10	FD05D	FD10D
Key Feature	High Speed and Low Capacitance in a TO-46 Can with a Ball Lens	High Speed and Low Capacitance in a Direct Fiber-Coupled FC/PC Package	High Speed and Low Capacitance	High Speed, High Responsivity, and Low Capacitance	Large Active Area and High Speed	High Speed and Low Dark Current	Long Wavelength Range	Long Wavelength Range and Large Active Area
Info								
Wavelength Range	800 - 1700 nm	900 - 1700 nm	900 - 2600 nm	900 - 2600 nm				
Active Area	0.01 mm ² (Ø120 µm)	0.01 mm ² (Ø120 µm)	0.018 mm ² (Ø150 µm)	0.196 mm ² (Ø0.5 mm)	3.1 mm ² (Ø2 mm)	0.79 mm ² (Ø1 mm)	0.20 mm ² (Ø0.5 mm)	0.79 mm ² (Ø1.0 mm)
Rise/Fall Time ^a	300 ps / 300 ps @ 5 V	300 ps / 300 ps @ 5 V	300 ps / 300 ps @ 1550 nm, 5 V	2.5 ns / 2.5 ns @ 5 V	25 ns / 25 ns @ 3 V	10 ns / 10 ns @ 5 V	17 ns / 17 ns @ 0 V	25 ns / 25 ns @ 0 V
NEP (W/Hz ^{1/2})	4.5 x 10 ⁻¹⁵ @ 1500 nm	4.5 x 10 ⁻¹⁵ @ 1500 nm	1.3 x 10 ⁻¹⁴ @ 1550 nm	2.0 x 10 ⁻¹⁴ @ 1550 nm	6.0 x 10 ⁻¹⁴ @ 1550 nm	2.5 x 10 ⁻¹⁴ @ 1550 nm, 5 V	5.0 x 10 ⁻¹³ @ 2300 nm	1.0 x 10 ⁻¹² @ 2300 nm
Dark	0.05 nA (Typ.)	0.05 nA (Typ.)	0.5 nA (Typ.)	6 nA (Typ.)	50 nA (Typ.)	1.1 nA (Typ.)	1 µA (Typ.)	3 µA (Typ.)

Current	@ 5 V	@ 5 V	@ 5 V	@ 5 V	@ 1 V	@ 5 V	@ 0.5 V	@ 0.5 V
Junction Capacitance	2.0 pF (Typ.) @ 5 V	2.0 pF (Typ.) @ 5 V	1.5 pF (Typ.) @ 5 V	10 pF (Typ.) @ 5 V	100 pF (Typ.) @ 3 V	80 pF (Typ.) @ 5 V	140 pF (Typ.) @ 0 V	500 pF (Typ.) @ 0 V
Package	TO-46	TO-46, FC/PC Bulkhead	TO-18	TO-46	TO-5	TO-5	TO-18	TO-18
Compatible Sockets	STO46S STO46P	STO46S STO46P	STO46S STO46P	STO46S STO46P	STO5S STO5P	STO5S STO5P	STO46S STO46P	STO46S STO46P

- τ_{eff} Typical Values; $R_L = 50 \Omega$ Unless Otherwise Specified

Part Number	Description	Price	Availability
FGA01	InGaAs Photodiode, 300 ps Rise Time, 800-1700 nm, Ø0.12 mm Active Area	\$62.76	Today
FGA01FC	InGaAs Photodiode, 300 ps Rise Time, 800-1700 nm, Ø0.12 mm Active Area, FC/PC Bulkhead	\$159.07	Today
FGA015	InGaAs Photodiode, 300 ps Rise Time, 800-1700 nm, Ø150 µm Active Area	\$58.35	Today
FDGA05	InGaAs Photodiode, 2.5 ns Rise Time, 800-1700 nm, Ø0.5 mm Active Area	\$148.25	Today
FGA21	InGaAs Photodiode, 25 ns Rise Time, 800-1700 nm, Ø2 mm Active Area	\$241.31	Today
FGA10	InGaAs Photodiode, 10 ns Rise Time, 900-1700 nm, Ø1 mm Active Area	\$180.71	Today
FD05D	InGaAs Photodiode, 17 ns Rise Time, 900-2600 nm, Ø0.5 mm Active Area	\$127.69	Today
FD10D	InGaAs Photodiode, 25 ns Rise Time, 900-2600 nm, Ø1.0 mm Active Area	\$226.17	Today

[Hide Dual Band Si/InGaAs Photodiode](#)

Dual Band Si/InGaAs Photodiode

- ▶ Dual Detector Chip Design - Si Over InGaAs - Provides Wide Detector Range
- ▶ 4-Pin TO-5 Package
- ▶ Large Active Area

Item #	Info	Wavelength Range	Active Area	Package	Rise/Fall Time ^a	NEP (W/Hz ^{1/2})	Dark Current	Junction Capacitance	Compatible Sockets
DSD2		400 - 1100 nm (Si) 1000 - 1800 nm (InGaAs)	5.07 mm ² (Ø2.54 mm, Si) 1.77 mm ² (Ø1.50 mm, InGaAs)	TO-5	4.0 µs (Both Layers) @ 0 V	1.9 x 10 ⁻¹⁴ (Si) 2.1 x 10 ⁻¹³ (InGaAs)	1 nA @ 1 V (Si) 0.5 nA @ 1 V (InGaAs)	450 pF @ 0 V (Si) 300 pF @ 0 V (InGaAs)	Not Available

- τ_{eff} Typical Values; $R_L = 50 \Omega$ Unless Otherwise Specified

Part Number	Description	Price	Availability
DSD2	Dual Band Si/InGaAs Detector, 4 µs Rise Time, 400 - 1700 nm, Ø2.54/Ø1.5 mm	\$604.91	Today

[Hide Ge Photodiodes - NIR Wavelengths](#)

Ge Photodiodes - NIR Wavelengths

Click Image for Details				
Item #	FDG03	FDG05 ^a	FDG50	FDG10X10
Key Feature	Large Active Area in a TO-5 Can	High Speed on a Ceramic Substrate	Large Active Area in a TO-8 Can	Largest Active Area
Info				
Wavelength Range	800 - 1800 nm	800 - 1800 nm	800 - 1800 nm	800 - 1800 nm
Active Area	7.1 mm ² (Ø3 mm)	19.6 mm ² (Ø5 mm)	19.6 mm ² (Ø5 mm)	100 mm ² (10 mm x 10 mm)

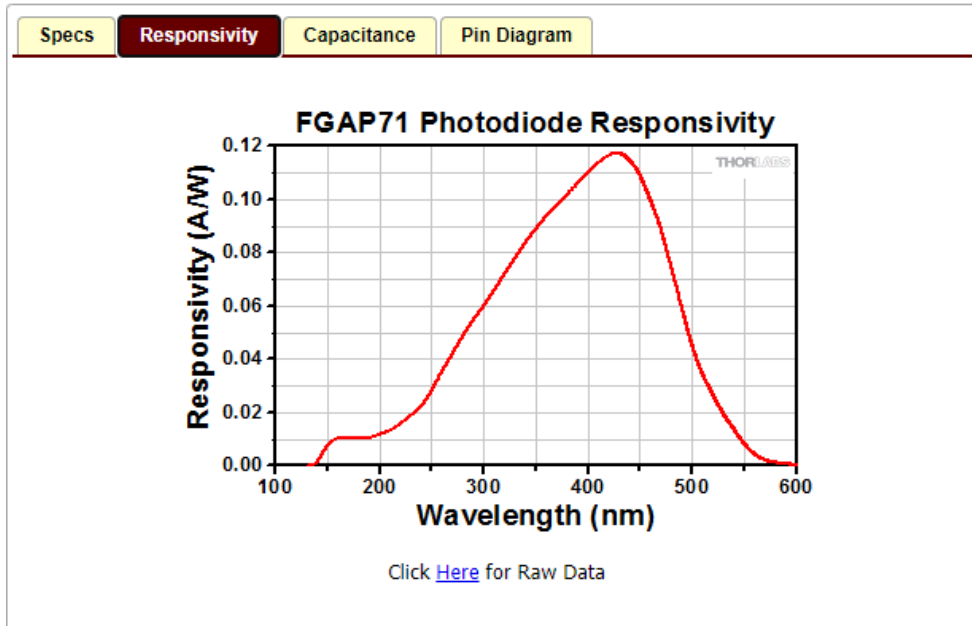
Rise/Fall Time ^b	600 ns / 600 ns @ 3 V	220 ns / 220 ns @ 3 V	220 ns / 220 ns (Typ.) @ 10 V	10 μ s (Typ.) @ 1 V
NEP	2.6×10^{-12} W/Hz ^{1/2} @ 1550 nm	4.0×10^{-12} W/Hz ^{1/2} @ 1550 nm	4.0×10^{-12} W/Hz ^{1/2} @ 1550 nm	4.0×10^{-12} W/Hz ^{1/2} @ 1550 nm ^c
Dark Current	4.0 μ A (Max) @ 1 V	40 μ A (Max) @ 3 V	60 μ A (Max) @ 5 V	50 μ A (Max) @ 0.3 V
Junction Capacitance	6 nF (Typ.) @ 1 V 4.5 nF (Typ.) @ 3 V	3000 pF (Typ.) @ 3 V	1800 pF (Max) @ 5 V 16000 pF (Max) @ 0 V	80 nF (Typ.) @ 1 V 135 nF (Typ.) @ 0 V
Shunt Resistance	25 k Ω (Min)	-	4 k Ω (Typ.)	2 k Ω (Min)
Package	TO-5	Ceramic	TO-8	Ceramic
Compatible Sockets	STO5S STO5P	Not Available	STO8S STO8P	Not Available

- ~~ad~~ Please note that the wire leads on the FDG05 and FDG10X10 are attached to the sensor using a conductive epoxy, as soldering them on would damage the sensor. This results in a fragile bond. Care should be taken while handling this unit so that the wire leads are not broken.
- ~~ab~~ Typical Values; R_L = 50 Ω Unless Otherwise Specified
- ~~ac~~ NEP is Specified for the Photovoltaic Mode

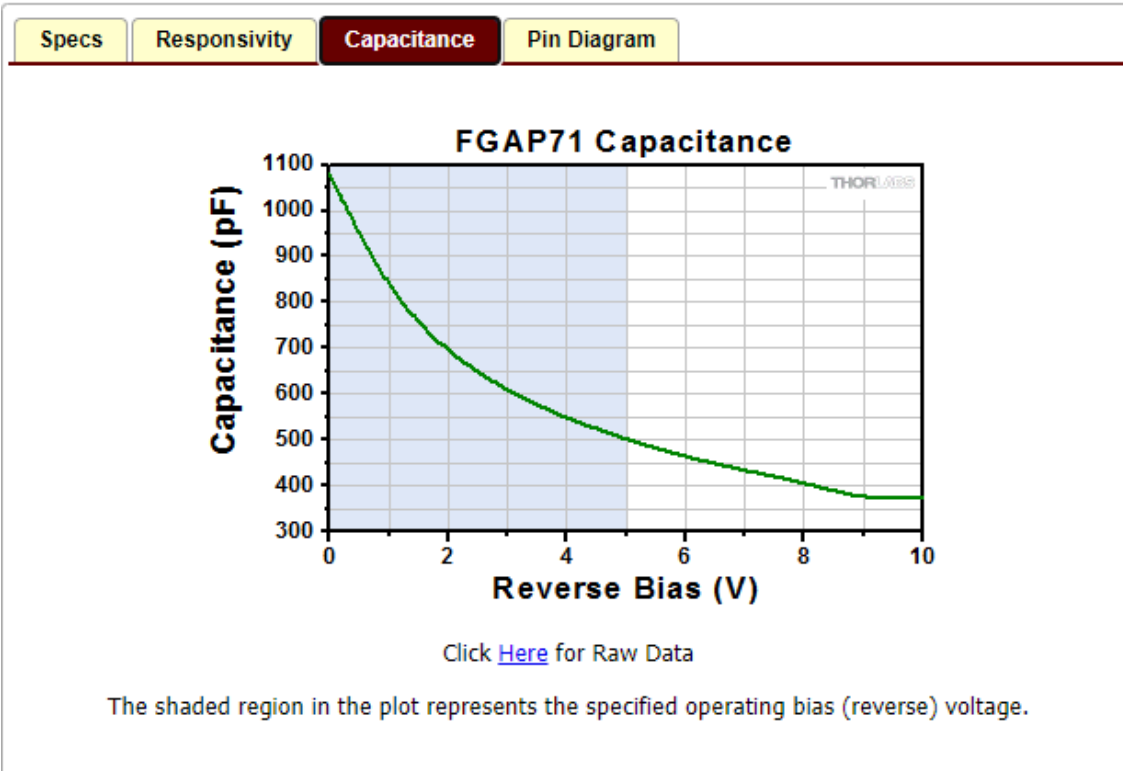
Part Number	Description	Price	Availability
FDG03	Ge Photodiode, 600 ns Rise Time, 800 - 1800 nm, \varnothing 3 mm Active Area	\$138.51	Today
FDG05	Ge Photodiode, 220 ns Rise Time, 800 - 1800 nm, \varnothing 5 mm Active Area	\$264.04	Today
FDG50	Ge Photodiode, 220 ns Rise Time, 800 - 1800 nm, \varnothing 5 mm Active Area	\$293.25	Today
FDG10X10	Ge Photodiode, 10 μ s Rise Time, 800 - 1800 nm, 10 mm x 10 mm Active Area	\$498.62	Today

Specs	Responsivity	Capacitance	Pin Diagram
Specifications			
Sensor Material	GaP		
Wavelength Range	150 - 550 nm		
Peak Wavelength	440 nm		
Responsivity	0.12 A/W		
Active Area Diameter	4.8 mm ² (2.2 mm x 2.2 mm)		
Rise/Fall Time (R _L = 50 Ohms, 5 V, 440 nm)	55 ns / 55 ns		
NEP, Typical (440 nm, 5 V)	1.3 x 10 ⁻¹⁴ W/Hz ^{-1/2}		
Dark Current (5 V)	15 pA (Typ.) 40 pA (Max)		
Capacitance (0 V)	1000 pF (Typ.)		
Package	TO-39		
Maximum Rating			
Max Bias (Reverse) Voltage	5 V		
Reverse Current	2 mA		
Operating Temperature	-40 to 125 °C		
Storage Temperature	-40 to 125 °C		

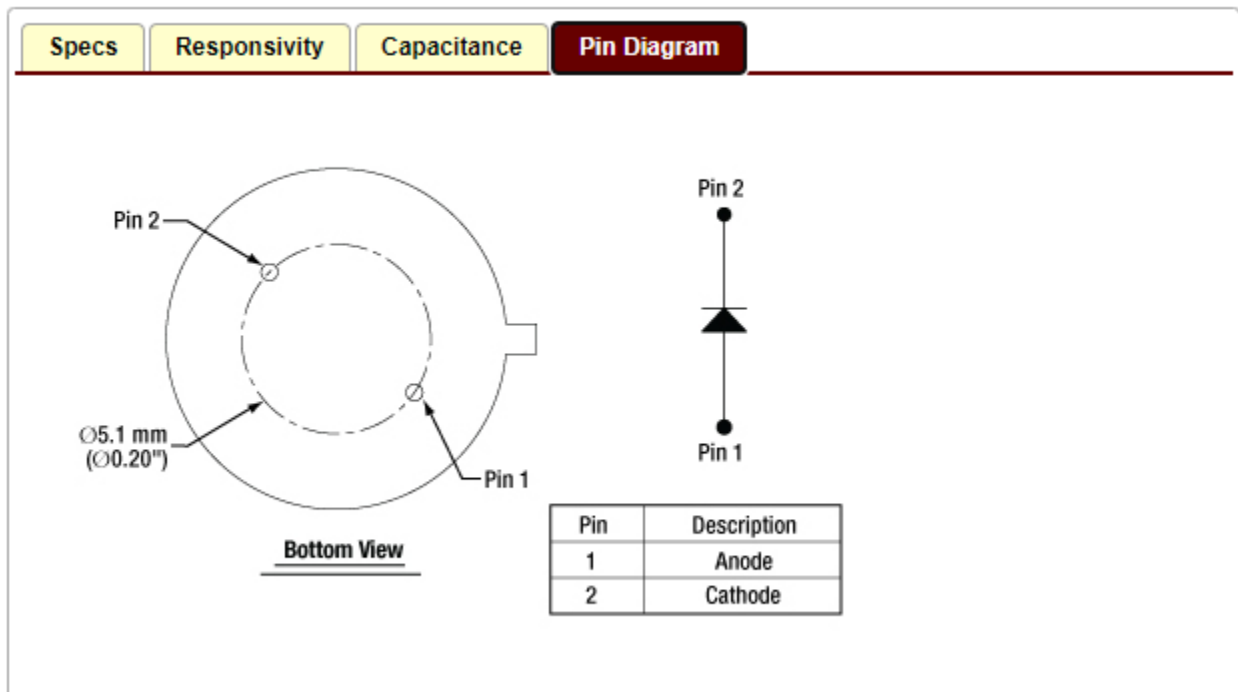
Based on your currency / country selection, your order will ship from Newton, New Jersey



Based on your currency / country selection, your order will ship from Newton, New Jersey



Based on your currency / country selection, your order will ship from Newton, New Jersey



Based on your currency / country selection, your order will ship from Newton, New Jersey

